LHCb note 2003-075

Measurements of Prototype Ladders for the Silicon Tracker with a Laser.

R. P. Bernhard, C. Lois*, St. Heule , M. Needham, A. Vollhardt
Physik-Institut der Universität Zürich

D. Volyanskyy
National Taras Shevchenko University of Kiev

July 18, 2003

Abstract

Results of measurements made with in a laser test-stand on prototype ladders for the LHCb Silicon tracker are discussed in detail.

*On leave from Universidad de Santiago de Compostela

1 Introduction

The LHCb Silicon Tracker (ST) project consists of two sub-detectors that will be built using silicon micro-strip technology. The first sub-detector is the inner part of the tracking stations T1-T3. The 'Inner Tracker' (IT) will cover a cross-shaped area around the beam-pipe in each of these stations. Research and development for the IT and the resulting technical design are described in [1].

The second sub-detector is the the so-called 'Trigger Tracker' (TT). This consists of four layers of silicon located upstream of the magnet. The decision to construct the TT station entirely from silicon micro-strip technology was taken in May 2002. Further R+D is necessary to verify the design concept for this station. In particular the forseen design has ladders of 33 cm in length. The longest ladder tested so far for the Inner Tracker was 22 cm long and 320 μm thick. It was found to give a S/N performance that was just acceptable. On the other hand the latest generation of the front-end chip — the Beetle 1.2 is expected to give better S/N performance compared to the Beetle 1.1 that was used in the previous studies [2]. Five prototype ladders have been constructed in order to study the performance with the Beetle 1.2 and to determine the optimal wafer thickness for the TT sensors. The relevant properties of the ladders are summarized in Table. 1. The total strip capacitances, C_{Strip}, have been calculated using the numbers in [3].

Ladder	Strip length/cm	Nominal thickness/μm	Pitch/μm	Metal strip width/μm	C_{Strip}/pF
LHCb1	10.8	320	198	78	16.8
LHCb2	21.6	320	198	78	33.6
LHCb3	32.4	320	198	78	50.6
GLAST	26.3	410	228	62	41.3
CMS	28.9	500	183	58	37.6

Table 1: Prototype ladder properties. The numbers quoted for the LHCb multi-geometry sensors are for Region C.

First tests on these ladders have been made in a laser test-stand at the University of Zürich. Such setups have been widely used in the design and construction of silicon detectors [4, 5, 6] and have several advantages. They are relatively easy to construct and allow fast characterization of the performance of both the silicon sensor and the front-end electronics. In addition,

the laser spot can be positioned on very specific regions of the sensor allowing studies to be made of the strip-to-strip uniformity, charge sharing and capacitive coupling between adjacent readout strips. On the other hand the laser set-up has some drawbacks. First, the stability of the laser diode with time and temperature must be monitored. Second, care must be taken to avoid internal reflection of the laser signal from the aluminium backplane. In addition, the laser pulse cannot penetrate the metallization of the readout strip. This means it is not possible to make measurements in this region of the detector. Finally, no measurement of cluster finding efficiency is possible in the laser setup since the absolute charge scale is uncertain.

It should also be noted that the charge distribution created by the laser pulse is not the same as that created by a charged particle. Ignoring δ-rays the charge distribution due to a charged particle is uniform. The laser produces an exponentially decreasing charge density

$$\frac{dQ}{dz} \propto e^{-\frac{y}{a(\lambda)}}$$

where $a(\lambda)$ is the penetration depth. The wavelength of the laser used is 1064 nm which corresponds to a penetration depth of 400 μm [5]. In Fig. 1 the expected charge distributions produced by the laser, calculated assuming that there is no reflection from the backplane, are compared to those due to a charged particle. It can be seen that for the LHCb ladders the laser is a reasonable approximation to a charged particle. This statement is less true for the thicker GLAST and CMS ladders.

In this note the results of the studies made with the laser are described. A comprehensive measurement program consisting of:

- Functionality tests
- Charge calibration
- Delay scans
- HV scans
- Position scans

was carried out. Around two million triggers were recorded in a period of four weeks.

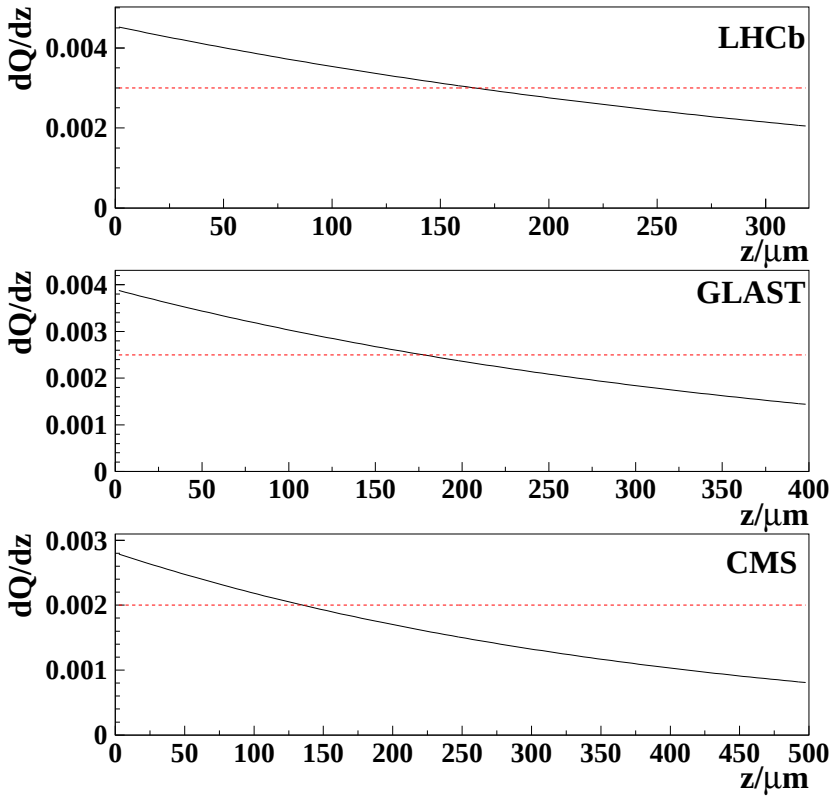

Figure 1: Comparisons of charge density distributions for a charged particle (dotted line) and the laser (solid line). All the curves are normalized to unit area.

2 Setup

An overview over the laser setup is shown in Fig. 2. To avoid daylight on the photosensitive silicon sensors, the test-ladders are mounted in a freezer, which also houses the stepper motor and the laser focusing optics which are described in Section 2.1. This also has the advantage of providing good thermal insulation for the detectors and gives a stable temperature inside the box. The readout hybrid of the test ladder was mounted on a water cooled copper block. The temperature off the coolant was kept at 12°C during the measurement program. Two PT100 temperature sensors were used to monitor the ambient temperature inside the box and the temperature of the cooling block. The temperature was (20.9 ± 0.2)°C inside the box and (13.3 ± 0.1)°C on the cooling block. A 40 MHz oscillator was used as system clock. The trigger rate was around 20 Hz.

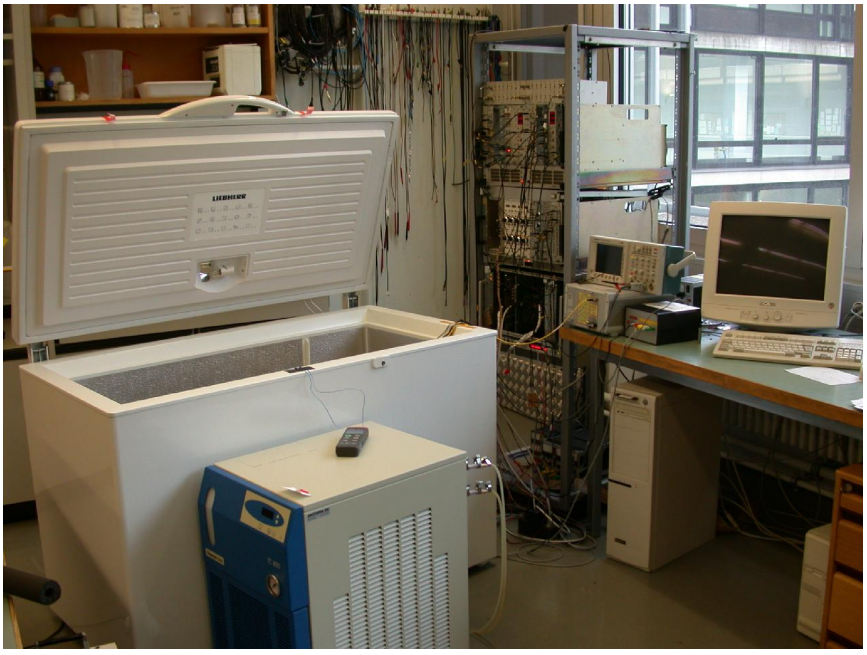

Figure 2: Overview of the laser test-stand setup

2.1 Laser and stepper motor

A 1064 nm Nd:YAG laser diode [1] was used to produce a signal in the silicon. This wavelength gives a photon energy of 1.165 eV which is large enough to reach the band gap of silicon (E_G = 1.1 eV at T = 300 K). These photons then create electron hole pairs which drift to backplane respectively readout strips generate the sensor current. The laser is pulsed with a pulse generator with a rise time of ≈2 ns. The pulse generator is triggered by the readout trigger an adjustable delay time between laser pulser and sampling time of the readout chip allows to perform delay scans. The height of the laser signal is determined by the amplitude of the pulse but is not linear with the input voltage. In fact there is a lower edge, below which no signal can be seen. Operating the laser close to this edge results in large instabilities. Therefore a high value for the input voltage was chosen and a passive beam splitter was used to attenuate the laser signal. The signal height was adjusted to deliver an ADC signal corresponding to approximately one MIP [2]. The height of the laser signal was found to drift with time. After a measuring period of $\sim$ 2 hours fluctuations of the signal height of order $\sim$ 5% were observed. To reduce this problem the laser was turned off periodically and allowed to cool.

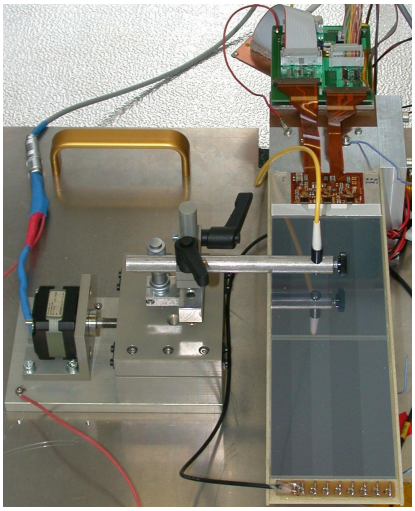

Figure 3: Inside view of the freezer. On the left side the stepper motor with the optical unit, in the top part the readout electronics and under the stepper motor arm a test ladder is visible.

The laser beam is guided via optical fibres from the beam splitter to the optical focusing unit. The shell of the optical unit is fixed in a height adjustable arm of the sledge (see Fig. 3). According to the laser optics specifications the focal point is 12 mm in front of the lensing system. This height of the arm above the silicon sensor can be adjusted with a micrometer screw in order to

[1] The laser system was produced by M. Glaser from the CERN EP-Divison.

[2] As a reference the height of a one MIP signal for each ladder from the charge calibration, as explained in Section 4, was used.

focus the laser beam.

The stepper motor is controlled through a LabVIEW program. The axis of the motor is connected via a thread rod with the sledge on which the optical unit of the laser is mounted (see Fig. 3). The stepper motor is mounted into the test system in such a way, that the optical unit can be moved perpendicular to the strips of the test sensors. The step size of the stepper motor is 5 μm.

2.2 Readout Chain

The sensors are wire bonded to a readout hybrid which holds the three Beetle 1.2 chips [7]. The readout mode of the chips used was 128 analogue channels multiplexed onto one port at 40 MHz. The output signals from the Beetle chips are connected via a 9 cm long Kapton flex cable to a PCB board. On this board the signals are multiplexed and transfered via a 5 m long twisted pair CAT6-cable out of the box. In the other direction the differential control signals (clock, trigger, reset) are transmitted to the Beetle hybrid. The PCB also contains connectors for the high and low voltage which are supplied from power supplies outside the freezer. The low voltage is needed for operation of the Beetle chip and the high voltage is used to bias the sensors. Outside the box the CAT6 cable is connected to an interface which de-multiplexes and amplifies the signals of the three Beetle chips for the following digitization stage. This is carried out by 8-bit FADCs that are located on an ODE prototype board [8]. The ODE board is read out via the VME bus to a PC running a LabVIEW program.

The programming of the Beetle readout chips was performed using with a standard I^2C interface. That was controlled via a LabVIEW program provided by the ASIC Lab in Heidelberg. In particular it should be noted that it is possible to change the shaping time of the Beetle chip within a certain range by setting different values of the parameter Vfs. Tests were performed using values of Vfs set to 0 mV, 400 mV and 1000 mV where a value of 0 mV corresponds to the fastest shaping.

To process and analyse the data a modified version of the software developed for the ST test-beam was used. Details on the procedure used for determining pedestals and common mode noise can be found in [9].

3 Functionality Tests

Each ladder was checked for broken Beetle chips and disconnected channels. One Beetle chip on the LHCb1 ladder and one chip on the LHCb2 ladder did not work. The first failure was due to an accident during the installation of this ladder and was not repairable, the second was due to a disconnected power bond and was later fixed. Two bad bonds were found and repaired on the LHCb1 ladder.

A search was performed for noisy channels. As an example Fig. 4 shows the RMS of the noise in ADC counts versus channel number for the 384 channels on the CMS ladder. The channels bonded for calibration (Section 4) were found to be more noisy and are masked off in this plot. It can be seen that:

- Channels 123 and 124 are noisy.
- There is a tendency for either the first or the last channel on a Beetle chip to be noisy.

The second point was also found to be true for the other ladders tested. The results of the functionality tests are summarized in Table 2.

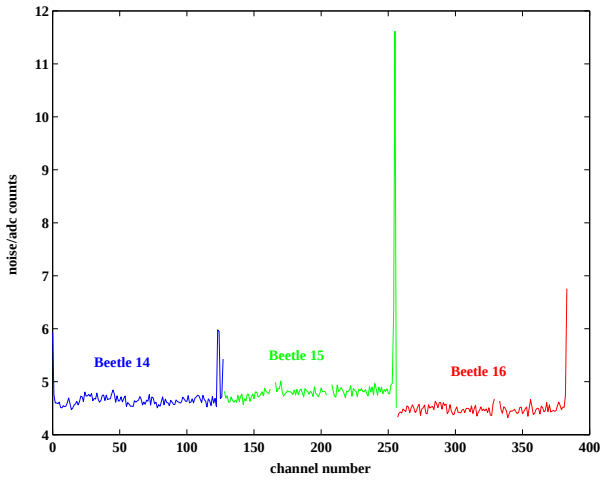

Figure 4: Channel noise for the CMS ladder, Vfs = 400 mV.

IV curves were measured for each ladder. These are shown in Fig. 5. The leakage currents for all the ladders are reasonably low up to the highest voltage tested and no breakdown was observed.

Ladder	Beetle ID	Working	First channel	Last channel	Other noisy channels
LHCb1	B	OK	Noisy	Noisy	—
LHCb1	C	OK	Noisy	Noisy	—
LHCb1	D	Destroyed	—	—	—
LHCb2	E	OK	Noisy	Noisy	—
LHCb2	F	OK	Noisy	OK	—
LHCb2	10	Disconnected Power Bond	—	—	—
CMS	14	OK	Noisy	Noisy	123,124
CMS	15	OK	OK	Noisy	—
CMS	16	OK	OK	Noisy	—
GLAST	17	OK	Noisy	OK	—
GLAST	18	OK	Noisy	OK	—
GLAST	19	OK	Noisy	Noisy	—
LHCb3	1A	OK	Noisy	Noisy	—
LHCb3	1B	OK	OK	OK	—
LHCb3	1C	OK	OK	Noisy	—

Table 2: Summary of functionality tests.

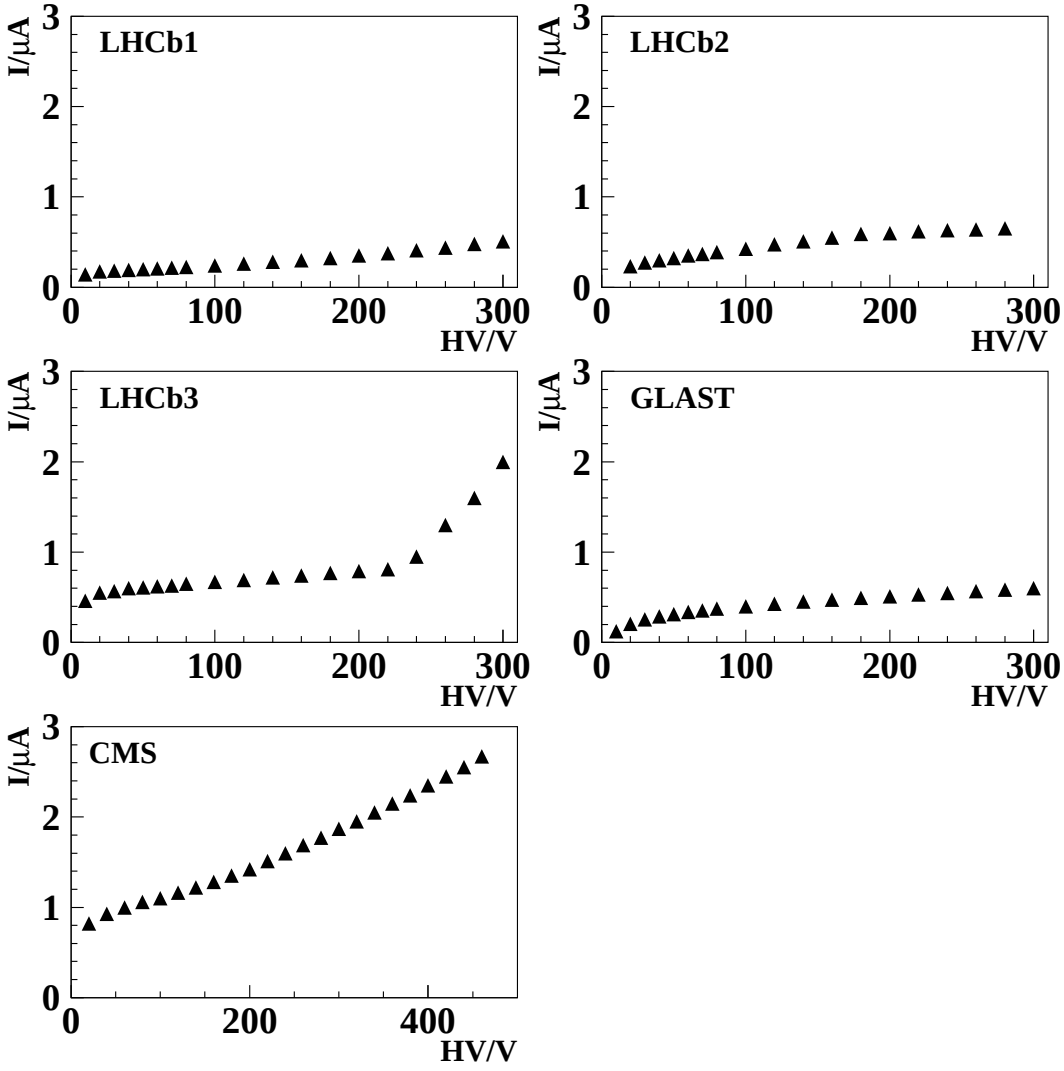

Figure 5: IV curves for the five ladders.

4 Charge Calibration

Using the laser set-up a charge calibration of the readout chain was performed. As will be seen the results of this are not fully understood. The procedure and results are described here for completeness but should be treated with caution.

The principle of the charge calibration is simple. Several selected channels are bonded to a PCB at the far end of the ladder with respect to the readout chip. The layout of the PCB is shown in Fig. 6. A pulser was used to put a

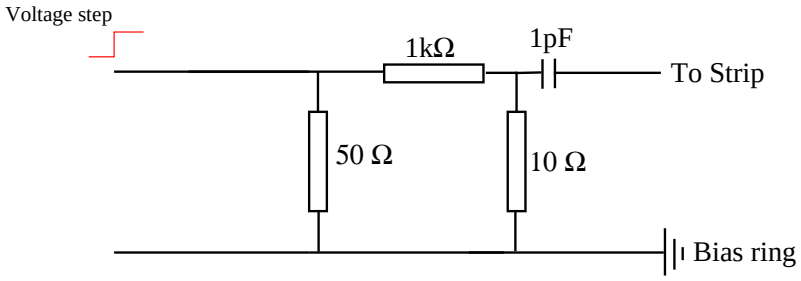

Figure 6: Calibration setup.

voltage step on the 1 pF capacitor. A voltage step of 350 mV creates then a charge of 22000 electrons on the readout strips bonded for calibration. The first step is to optimize the pulse time relative to the sampling time. To do this several runs were then taken varying the trigger delay around the rough position of the maximum. The optimal delay was then determined by fitting a parabola to the measured signal amplitudes as a function of delay time. With this setting several runs were taken varying the size of the voltage step. The observed number of ADC counts was then plotted versus the amplitude of the voltage step and a fit made to:

$$N_{ADC} = A_{off} + B_s \times V$$

The linearity of the data is illustrated in Fig. 7. It can be seen that the data is well described by a straight line. The size of A_{off} was found to vary from Beetle-to-Beetle but was at the level of 10 ADC counts or less for all the chips. The equivalent noise charge in electrons can then be extracted using:

$$ENC = \frac{22000 \times N_{ADC}(noise)}{350 \times B_s}$$

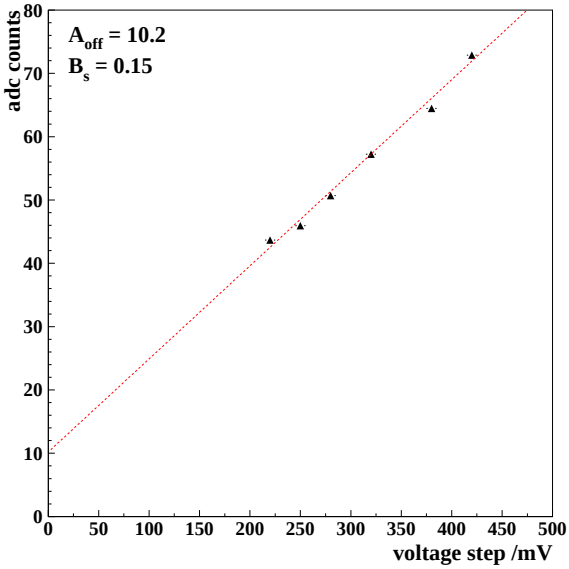

Figure 7: Calibration curve for Beetle 1A, channel 55, Vfs=0 mV.

where $N_{ADC}(noise)$ is determined from pedestals runs. In Fig. 8 the noise performance obtained for Vfs = 0 mV is plotted versus the measured capacitance of the ladders. The uncertainty on each point has two contributions:

- An uncertainty due to the averaging of several channels.
- A systematic uncertainty due to the correction for A_{off}.

These numbers can be compared to the results of front-end measurements with the Beetle 1.2 given in [1]. Those gave:

$$ENC = 450 + 47 \times C/pF$$

It can be seen in Fig. 8 that the measured points for the long ladders lie systematically below the values expected from the front-end measurements. If the measurements described here are correct it should result in significantly improved S/N performance for the long ladders.

A second calibration was attempted during the 2003 ST test-beam at the CERN SPS. The same procedure as above was used. In the test-beam it was observed that grounding the PCB via the bias ring as shown in Fig. 6 creates a current loop around the bias ring of the ladder and back through

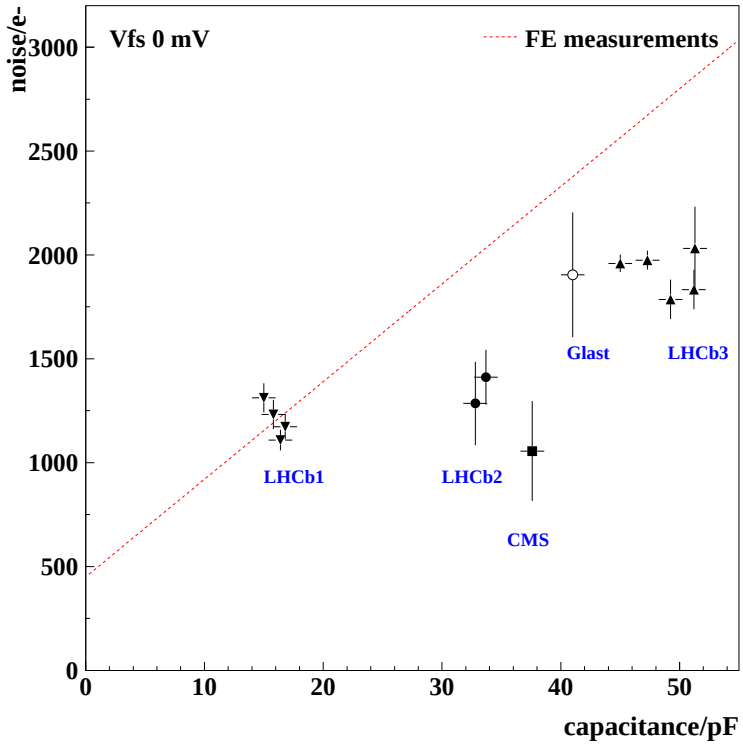

Figure 8: Equivalent noise charge versus Capacitance/pF, Vfs=0 mV.

the HV power supply. Very large signals were observed on the calibration channels which saturated the optical link used in the setup. To reduce this problem an additional connection to ground was made. Using this grounding scheme the calibration was repeated in the test-beam and similar results to those described here were obtained. The grounding problems that were observed may exist at a lower level in the setup described here. It should be noted that the procedure described above is robust against such problems. Nevertheless, in the near future it is planned to repeat the calibration with a better grounding scheme in the laser set-up.

5 Laser Focusing

One of the first steps in the measurement program for each ladder was to adjust the micrometer screw setting such that the focal point of the laser coincided with the centre of the sensor. The fact that the laser light does not penetrate the metallization of the readout strip can be used to achieve this as follows. First, the rough region of focus is defined by 'eye'. A scan is then made moving the laser spot across the sensor. An example of such a scan is shown in Fig. 9. It can be seen that as the position of the laser spot is moved there is an edge where the observed signal decreases rapidly to zero. This is the start of the metallization of the readout strip. A fit of an error function is made to this edge. This procedure is then repeated for several micrometer screw settings. The micrometer setting with the minimum 'σ' of the error

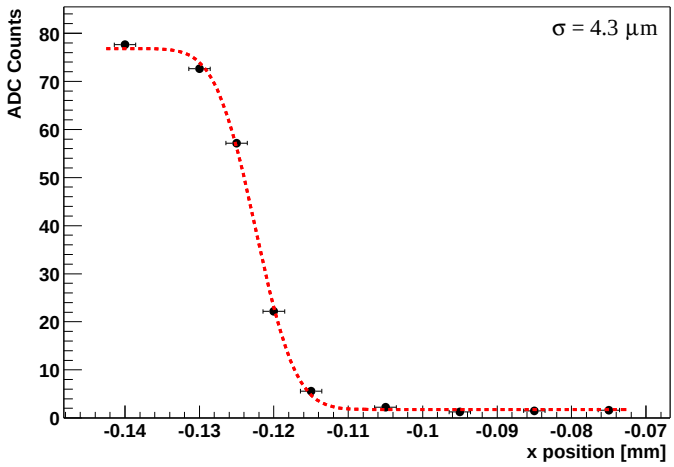

Figure 9: Example of a laser focussing run. A σ of 4.3 μm was achieved in this case.

function is taken as the optimal focus point. Typically, a 'σ' of 4 μm was achieved. This corresponds to a FWHM spot-size of 11 μm.

6 Delay scans

For each of the five ladders nine scans were made varying the delay between the trigger signal and the sampling time in order to investigate the dependence of the pulse shape on the bias voltage, shaping time and position of the laser spot. The conditions for the runs are summarized in Table 3. The

Run	Vfs/mV	High voltage	Position
1	400	V1	near strip
2	400	V1	mid strip
3	1000	V1	near strip
4	1000	V1	mid strip
5	0	V2	near strip
6	400	V2	near strip
7	400	V2	mid strip
8	1000	V2	near strip
9	1000	V2	mid strip

Table 3: Delay scans.

value of V1 for each ladder was chosen using the numbers given in [3] to be $20-30$V above the depletion voltage. The value of V2 was chosen to be well above the depletion voltage so as to guarantee full charge collection. The values of V1 and V2 are summarized in Table 4. It should be noted that the three sensors on the CMS ladders have quite different depletion voltages. The depletion voltage for the illuminated sensor was 190 V. The near strip data was taken at the edge of the metallization and the mid-strip equidistant between the centre of two readout strips.

Ladder	Depletion voltage/V	V1/V	V2/V
LHCb1	65	90	200
LHCb2	65	90	200
LHCb3	65	90	200
GLAST	70	95	235
CMS	130-220	220	385

Table 4: Chosen values of V1 and V2 for delay scans.

Two examples from the 45 delay scans that were taken are shown in Fig. 10 and Fig. 11. The first, Fig. 10 shows the results of a pulse shape scan with

the fastest shaping, Vfs = 0 mV for the LHCb1 ladder. The signal on the strip closest to that illuminated by the laser together with the two adjacent strips is shown. The signal on the adjacent strips can be reproduced in a simulation in which capacitive coupling between the readout strips is taken into account [10]. It can be seen that the signal on the right neighbour has a higher maximum value than the left. This is due to the fact that the laser is positioned closer to the right strip than to the left allowing some charge sharing to occur to this strip in addition to the capacitive coupling. If the other side of the strip was illuminated then the left neighbour was found to have a higher maximum value than the right. Fig. 11 shows a delay scan

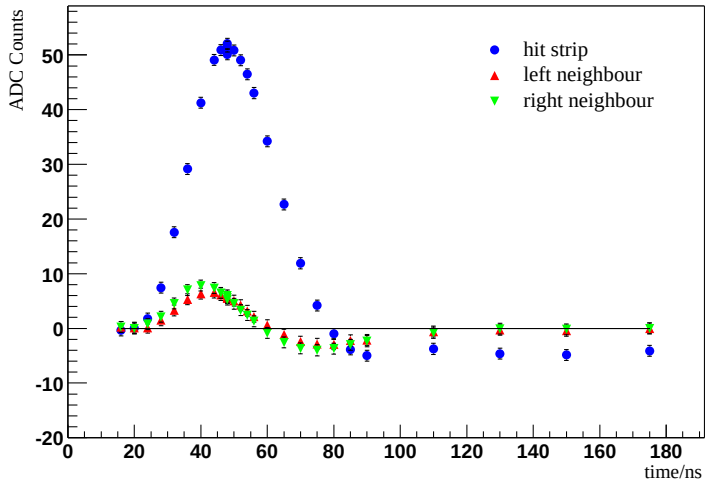

Figure 10: Delay scan for the LHCb1 ladder, HV = 200 V, Vfs = 0 mV, near strip.

with the slowest shaping, Vfs = 1000 mV for the LHCb3 ladder.

From each of the delay scans the following information can be extracted:

- Rise-time of the pulse
- Signal remainder after 25 ns on the readout strip illuminated by the laser, i.
- Relative size of the undershoot of the baseline.
- Properties of the signal induced by capacitive coupling on strip i+1.

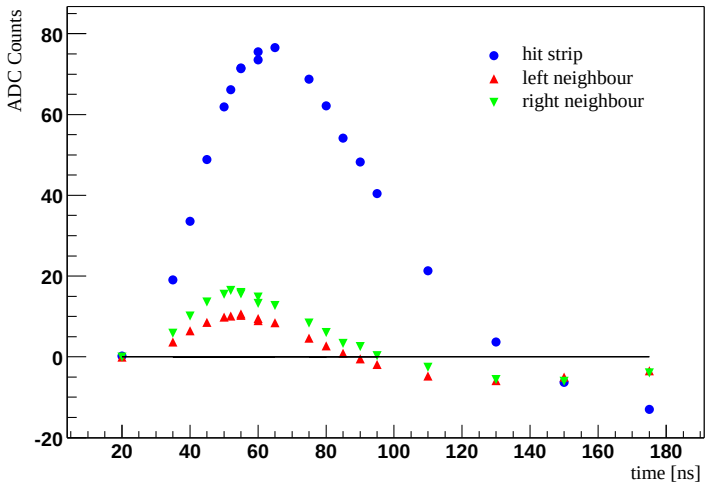

Figure 11: Delay scan for the LHCb3 ladder, HV = 200 V, Vfs = 1000 mV, near strip.

6.1 Signal Remainders

The LHC is designed to operate at a bunch crossing rate of 25 ns. Fast signals are therefore required in order to minimize the number of tracks from the previous bunch crossing that are reconstructed in a triggered event. A measure of the shaping time is the signal remainder after 25 ns. Monte Carlo studies of the LHCb detector performance assume a signal remainder of 0.3 for IT and 0.5 for TT [11].

The remainder was found not to depend significantly on either the bias voltage or the position of the laser relative to the strip. However, as expected a clear dependence is observed on the Beetle shaping parameter Vfs and the load capacitance. This can clearly be seen in Fig. 12. In Fig. 13 the results with Vfs=0 mV are compared to the Beetle 1.2 front-end measurements described in [1]. It can be seen that for the long ladders the measured remainder is systematically smaller than expected from the front-end measurements. It can also be seen that a remainder of less than 0.5 as is assumed in the LHCb Monte Carlo program for the TT station can easily be met for values of Vfs up to $\sim$ 400 mV.

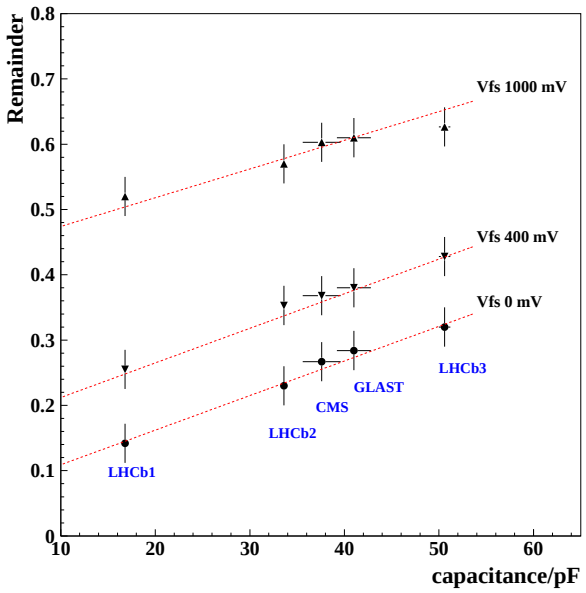

Figure 12: Remainder as a function of capacitance for various settings of Vfs. The dotted lines are to guide the eye.

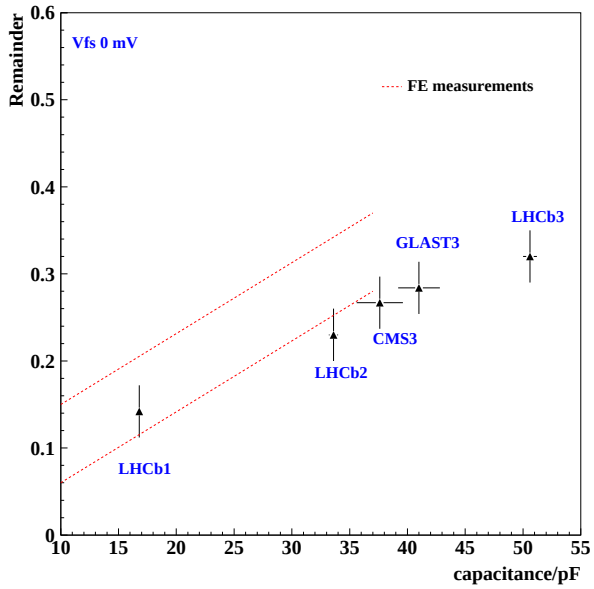

Figure 13: Comparison of the measured remainder with front-end measurements. The front-end measurements lie inside the dotted lines.

6.2 Rise-time

The rise-time is here defined as the time from 10% to 90% of the signal maximum. As expected, it was found to depend on the Beetle chip shaping parameter Vfs and the load capacitance. Fig. 14 shows the measured rise-times for the five ladders at the three Vfs settings.

Again, the results for Vfs=0 mV can be compared to the front-end measurements (Fig. 15). It can be seen that the measured rise-times are slightly slower than expected from the front-end measurements.

The effect of the bias voltage was also investigated. As can be seen in Fig. 16, the rise-time is faster for the higher bias voltage. This is due to the higher electric field in the sensor which results in faster charge collection.

Finally, the dependence of the rise-time on the position of the laser relative to the strip was studied. In Fig.17 rise-times for near and mid-strip data are compared. The rise-time is found to be faster for the mid-strip data. This observation is somewhat surprising. Naively, it would be expected that the rise-time for the mid-strip data should be slower than that for the near strip since the charge has to drift towards and be collected on the strip. The observed behaviour may be related to the properties of the shoulders discussed in Section 6.4. Assuming the shoulders can be modelled as in [11] it is expected hat the mid-strip signal on one of the two illuminated strips has a component due to capacitive coupling from the other strip. It can be seen from Fig. 10 and Fig. 11 that such a component would arrive earlier in time than the one due to charge collection, effectively making the signal faster and the rise-time shorter.

6.3 Undershoot

It can be seen from Fig. 10 and Fig. 11 that there is an undershoot of the baseline. This occurs around 100 ns after the signal maximum. The relative undershoot is defined as the absolute value of the maximum negative signal divided by the value of the maximum positive signal. The only parameter that the size of the undershoot was found to depend on was Vfs. Fig. 18 shows the relative undershoot for the five ladders at the three different Vfs settings for high voltage V2. In this plot, no difference between Vfs = 0 and 400 mV is observed. However, the undershoot for the slowest shaping (Vfs = 1000mV) is clearly larger than for the other ones.

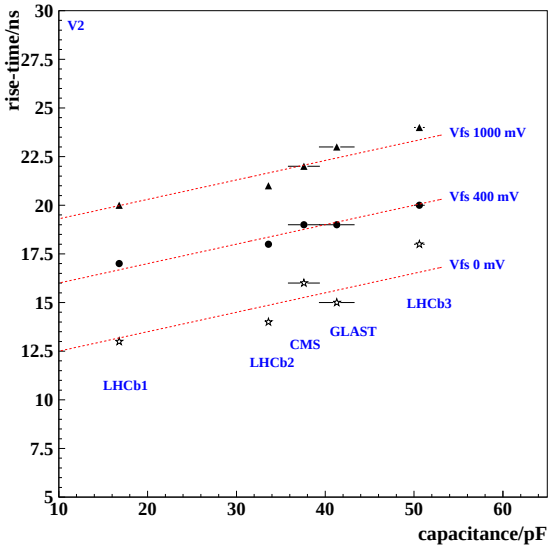

Figure 14: Rise-time for the five ladders, for three Vfs settings: 0, 400 and 1000 mV. The bias voltage was V2, and the laser was placed near strip. The error on each point is 2 ns.

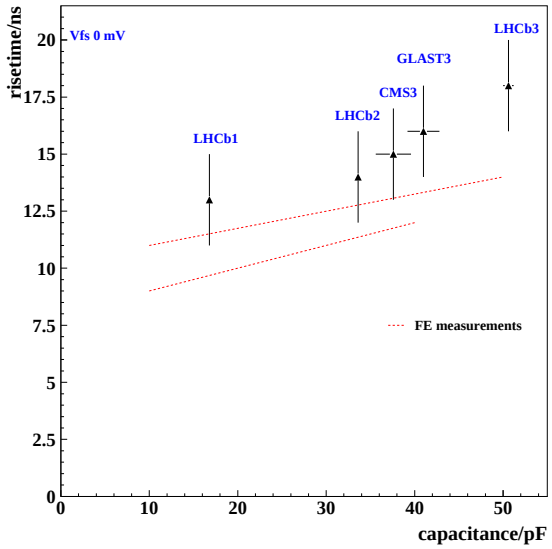

Figure 15: Comparison of rise-time for Vfs=0 mV, near strip V2 data with front-end measurements. The front-end measurements lie inside the dotted lines.

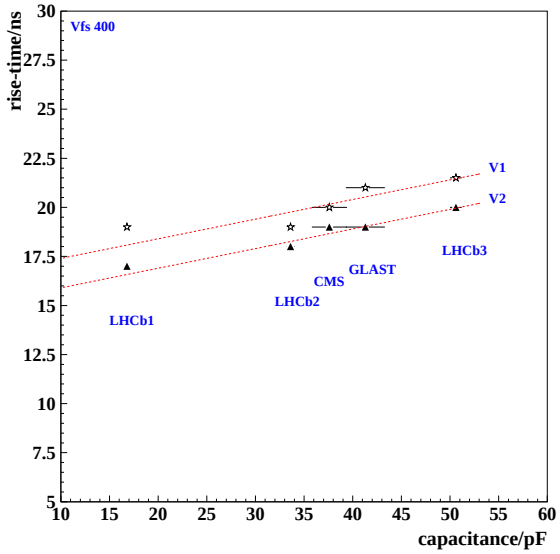

Figure 16: Rise-time as a function of the capacitance for the two bias high voltages. The laser position was near strip and Vfs = 400 mV. The error on each point is 2 ns.

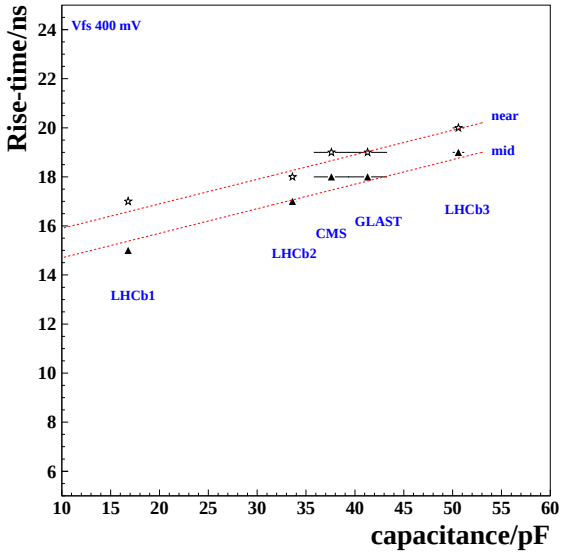

Figure 17: Comparison of the rise-time obtained with the laser placed near strip (near) and between two strips (mid). Vfs was set to 400 mV, and V2 was applied. The error on each point is 2 ns.

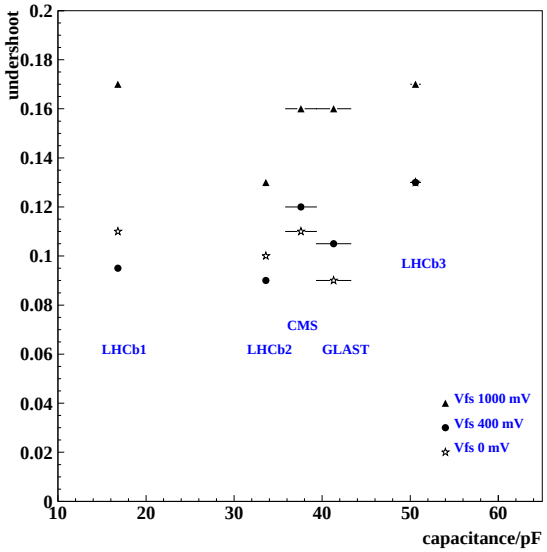

Figure 18: Relative size of the undershoot as a function of the capacitance for various settings of Vfs. The error on each point is 0.02.

6.4 Shoulders

It has been observed in tests with the previous generation of ST prototype ladders [9] that even if a charged particle passes through the centre of a strip, where no charge sharing can occur a significant signal is seen on the nearest neighbours of the strip. These 'shoulders' can be reproduced in a simulation that takes into account capacitive coupling between the readout strips [10]. The laser set-up is an ideal place to investigate the properties of the shoulders further.

It can be seen from Fig. 10 and Fig. 11 that the maximum amplitude for the shoulder occurs earlier in time than the maximum amplitude for the strip illuminated by the laser. This time difference, Δt(max) was found to depend neither on the bias HV nor the capacitance of the ladder. Some dependence on the shaping parameter Vfs is observed. It can be seen in Fig. 19 where Δt(max) versus Vfs/mV is plotted for the GLAST ladders, that Δt(max) increases with increasing Vfs. A similar trend was observed for the other ladders.

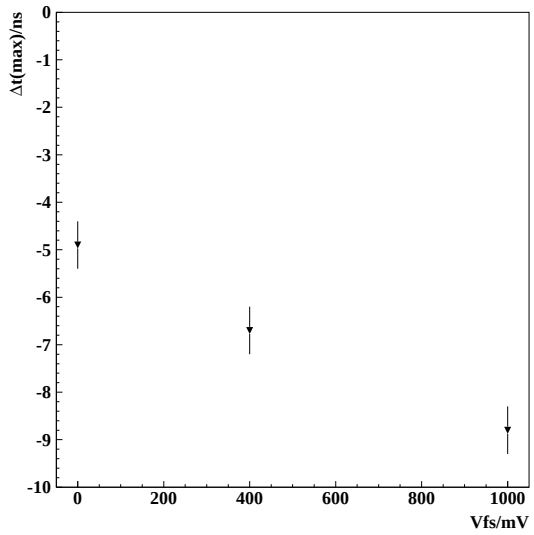

Figure 19: Δt(max)/ns vs Vfs/mV for the GLAST ladder, V2, near strip.

The relative maximum height of the shoulder, $\Delta_s(max)$ is defined as:

$$\Delta_s(max) = \frac{N_{ADC}(s)}{N_{ADC}(i)}$$

where $N_{ADC}(i)$ is the maximum signal in ADC counts on the illuminated strip and $N_{ADC}(s)$ is the maximum signal in ADC counts on the 'shoulder' strip. Both these values are estimated from parabola fits to the signal amplitude as a function of delay time for each distribution. The value of $\Delta_s(max)$ for each of the nine delay scans taken with the GLAST ladder is shown in Fig. 20. The most striking feature of this plot is the difference between the near strip and mid-strip data. The value of $\Delta_s(max)$ for the mid-strip data is significantly higher than for the near strip. It can also be seen that $\Delta_s(max)$ is slightly reduced as Vfs is increased. In addition the value of $\Delta_s(max)$ is smaller for the data taken with V2. Similar observations were made for the other four ladders tested. The results for the V2, Vfs 400 mV, near strip setting for the five ladders are summarized in Table 5. Very little dependence of the shoulder size on either the strip length or capacitance is observed.

Numbers for the relative size of the shoulder at the time of the maximum signal for the illuminated strip, Δ_s are also given in this Table. It can be seen that:

$$\Delta_s \approx 0.9 \times \Delta_s(max).$$

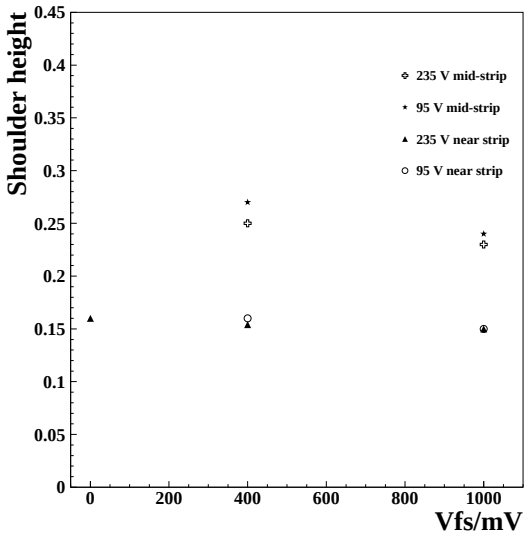

Figure 20: Relative maximum shoulder height for the GLAST ladder. The error on each point is 0.03

It also seems that the shoulders themselves have shoulders. This can be seen

Ladder	$\Delta_s(max)$	Δ_s
LHCb1	0.12 ± 0.03	0.11 ± 0.03
LHCb2	0.13 ± 0.03	0.11 ± 0.03
LHCb3	0.15 ± 0.03	0.14 ± 0.03
GLAST	0.15 ± 0.03	0.13 ± 0.03
CMS	0.18 ± 0.03	0.14 ± 0.03

Table 5: Values of $\Delta_s(max)$ and Δ_s for the five ladders, V2, Vfs = 400 mV, near strip data.

in Fig. 21 where in addition to the illuminated strip and its nearest neighbours the signal on the next neighbours is plotted. A small but significant signal with relative maximum height of 0.03 can clearly be seen on the next neighbours. No signal was observed on the next-to-next neighbours.

6.5 Charge deposition shapes

An alternative way to visualize the shoulders is to plot for a fixed trigger delay the average charge seen on the strips around the one illuminated by

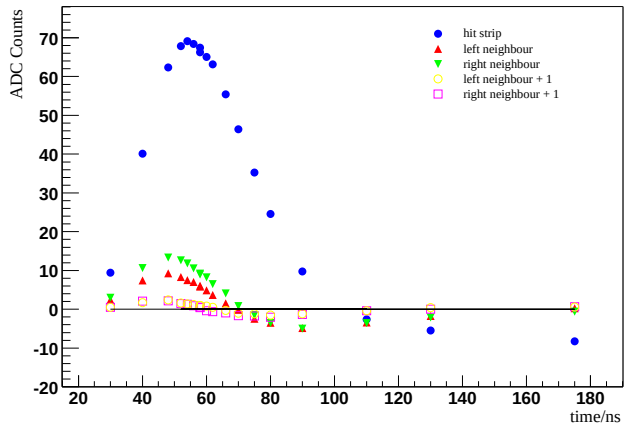

Figure 21: Delay scan for the LHCb2 ladder, V1, Vfs = 400 mV, on strip.

the laser. This has been done setting the trigger delay such that the signal on the strip closest to the laser spot is at its maximum value. Fig 22 shows the obtained shapes for the near strip data and Fig. 23 for the mid-strip data.

6.6 Summary

The delay scan data taken with the laser has provided a wealth of information. The dependence of the remainder on the shaping time has been investigated in detail. The results are found to be slightly better than expected from the front-end measurements. The measured rise-time for the near-strip data has been found to be slightly slower than expected. In addition it has been observed that the rise-time for the mid-strip data is *faster* than for the near strip data. The shoulders due to capacitive coupling have been studied in detail. It is has been been found that the maximum value for the shoulder is earlier in time than for the central strip. This observation may explain the faster rise-time for the mid-strip data. It has also been observed that the relative size of the shoulder is different for the near and mid-strip data.

To understand the data further simulation studies that model both the response of the silicon and the Beetle chip are being performed. The first results from such studies are described in [10].

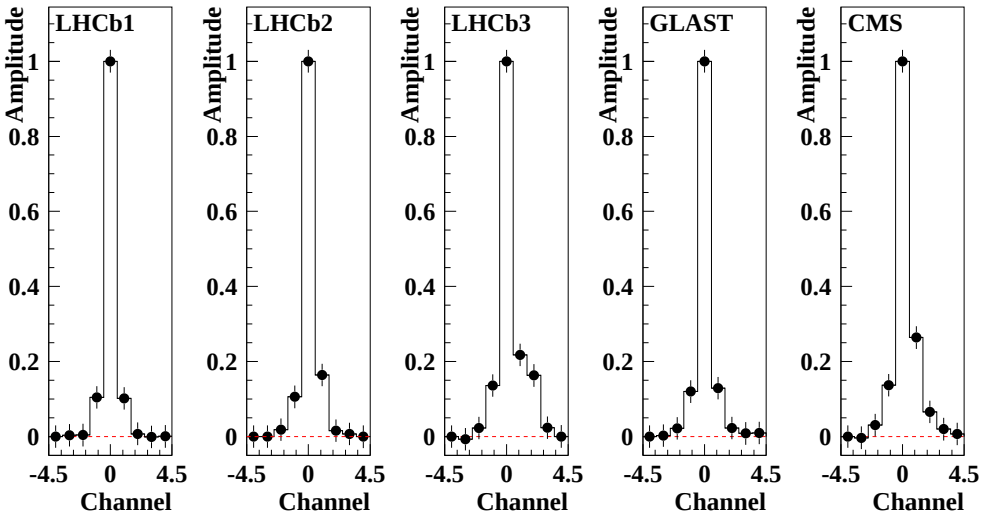

Figure 22: Charge depositions shapes for the near strip data, Vfs = 400 mV, V2. The amplitudes has been normalized such that the signal on the illuminated strip is one.

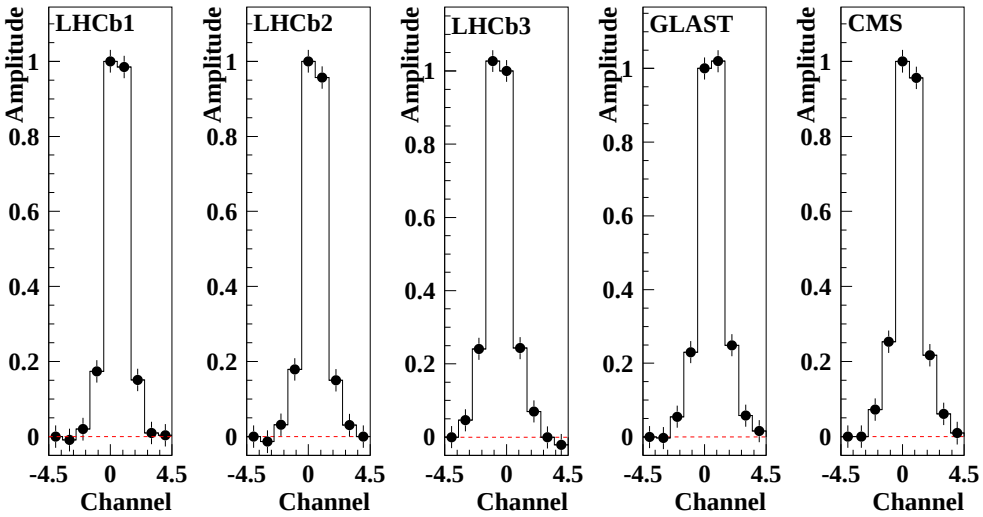

Figure 23: Charge depositions shapes for the mid-strip data, Vfs = 400 mV, V2. The amplitudes has been normalized such that the signal on the illuminated strip is one.

7 Bias voltage scans

For each of the five ladders a bias voltage scan was performed. It was shown in Section 6 that the time of the signal maximum depends on the applied bias voltage. Therefore for each bias voltage it was first necessary to determine the optimal delay setting. This was done by taking 4-5 runs chosen close to the best estimate of the optimal timing for the signal maximum and fitting a parabola to the measured signal as function of delay time. The dependence of the maximum signal amplitude (left) and the time dependence (right) of the signal maximal versus the applied bias voltage are shown in Fig. 24 to Fig. 28 for each ladder. All the measurements were performed with the Beetle shaping Vfs set to 400 mV and with the laser spot positioned close to the metallization of the readout strip.

The measurement showed that the LHCb1 sensor reaches the plateau at around 110 V. The other two ladders using LHCb sensors (LHCb2 sensor ladder and LHCb3 sensor ladder) reach the plateau a little bit earlier at around 100 V. For the GLAST ladder full charge collection starts at 150 V whereas for the CMS ladder this is the case at 440 V. Note also that for the CMS ladder the time of the maximum does not change up to 260 V (see Fig. 28).

Comparing the plateau voltages with the depletion voltages quoted in Table 4, and taking into account the different thicknesses of the sensors (see Table 1), one finds, that the obtained values are within the expectation for the GLAST ladder with a difference of 80 V. This is not valid for the CMS ladder. Here the difference between the measured depletion voltage and the bias voltage for full charge collection is 250 V. This and the dependence of the time of the signal maximum might be due to the fact, that the depletion voltages for two out of three sensors used for the test ladder differ by 90 V.

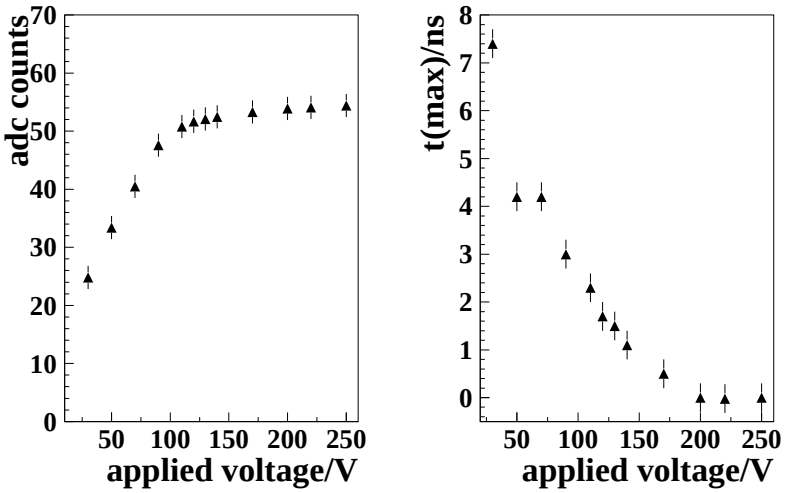

Figure 24: Dependence of the signal height (left) and the time of the maximum (right) versus the bias voltage for the LHCb1 ladder.

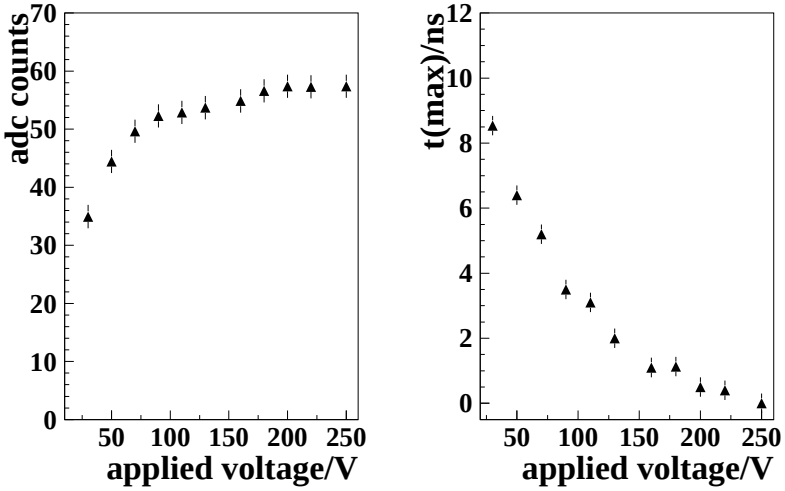

Figure 25: Dependence of the signal height (left) and the time of the maximum (right) versus the bias voltage for the LHCb2 ladder.

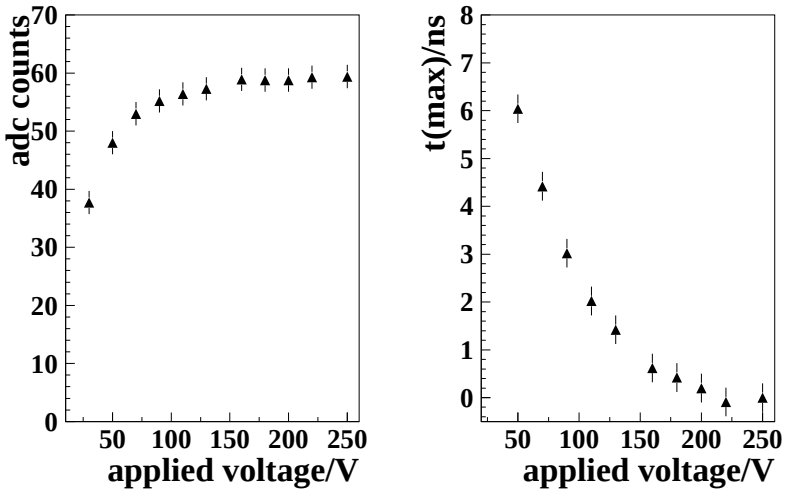

Figure 26: Dependence of the signal height (left) and the time of the maximum (right) versus the bias voltage for the LHCb3 ladder.

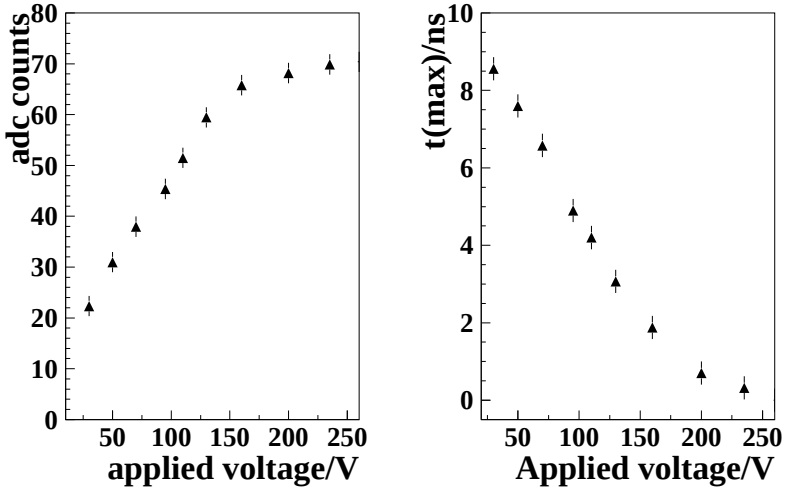

Figure 27: Dependence of the signal height (left) and the time of the maximum (right) versus the bias voltage for the GLAST ladder.

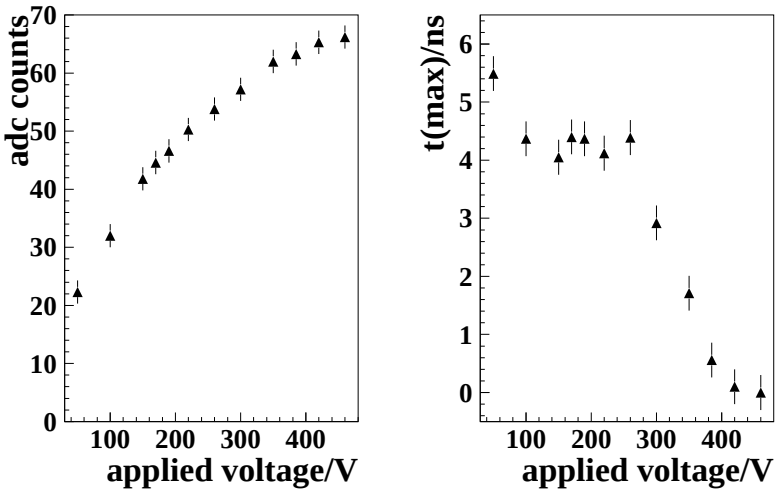

Figure 28: Dependence of the signal height (left) and the time of the maximum (right) versus the bias voltage for the CMS ladder.

8 Position scans

In tests performed with the previous generation of ST prototype ladders a charge loss of order $10 - 20\%$ was observed to occur in the region between two readout strips [1, 9]. The dependence of this charge loss on the bias voltage has been investigated in the laser set-up.

For each ladder two position scans were made, the first with the bias voltage set to V1 and the second with the bias voltage set to V2. The laser spot was moved across the strip by means of the step motor in steps of 5 μm. The results of these scans are shown in Fig. 29 to 33 for the five ladders. In each plot the signal on the left and right strips is shown together with the sum of the charge on the four strips closest to the laser position. In all plots the charge loss in the inter-strip region is clearly visible. In addition it can be seen that the total collected charge for the V2 data is always higher than for the V1. This is consistent with the results of Section 7 — full charge collection efficiency is not expected for the V1 bias voltage. It can also be seen that the left-hand side of each plot is generally higher than the right. This is due to the laser instabilities mentioned in Section 2. This effect is most pronounced for the data taken with the GLAST ladder (Fig. 32).

In the case of the GLAST plot, the worst example, the effects of laser instability can also be seen from the fact that the left-hand side of the plot is clearly higher than the right.

The following procedure was used to estimate the size of the charge loss. The average of the data taken near to the left and right strip was taken as a measure of the near strip charge. The uncertainty on this number was taken to be the difference between the left and right strip values divided by two. The charge mid-strip was taken as the value observed at the position midway between the left and right strips. The relative charge loss, Δ_q is then estimated as:

$$\Delta_q = \frac{N_{ADC}(near) - N_{ADC}(mid)}{N_{ADC}(near)}$$

Table 2 summarizes the results of the measurements of the charge loss for the two applied bias voltages.

In summary, a charge loss between the readout strips can clearly be observed for all ladders. However, the stability of the laser is not sufficient to make quantitative statements concerning for example the dependence of the dip on the bias voltage.

Ladder	Δ_q for V1 [%]	Δ_q for V2 [%]
LHCb1	17.5 ± 0.9	20.2 ± 1.3
LHCb2	17.4 ± 1.4	20.5 ± 1.1
LHCb3	11.6 ± 1.6	18.0 ± 1.2
GLAST	23.5 ± 6	24.2 ± 3
CMS	11.3 ± 1.6	10.5 ± 1.3

Table 6: Values of the relative charge loss, Δ_q for all the ladders. Vfs was set to 400 mV.

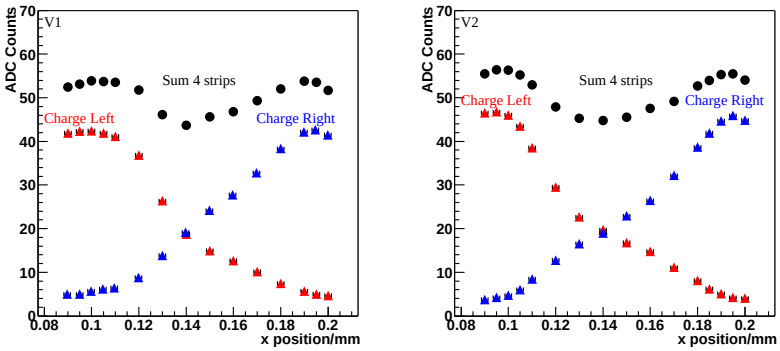

Figure 29: Charge sharing and loss for the LHCb1 ladder, Vfs = 400 mV.

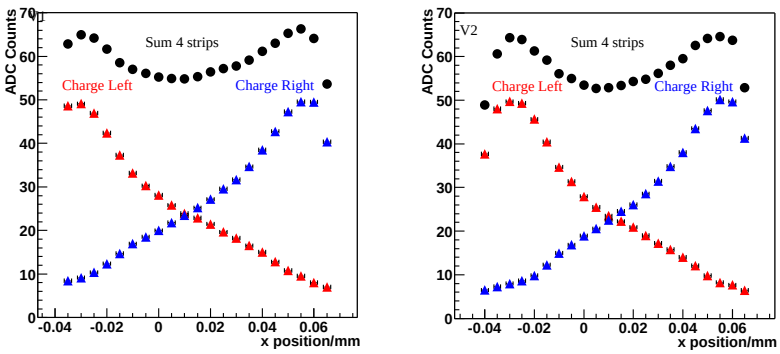

Figure 30: Charge sharing and loss for the LHCb2 ladder, Vfs = 400 mV.

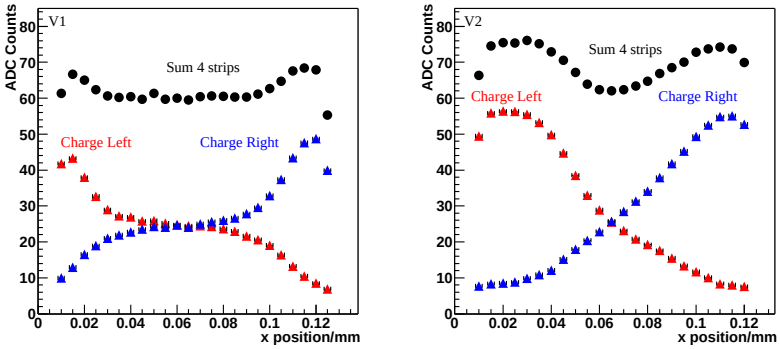

Figure 31: Charge sharing and loss for the LHCb3 ladder, Vfs = 400 mV.

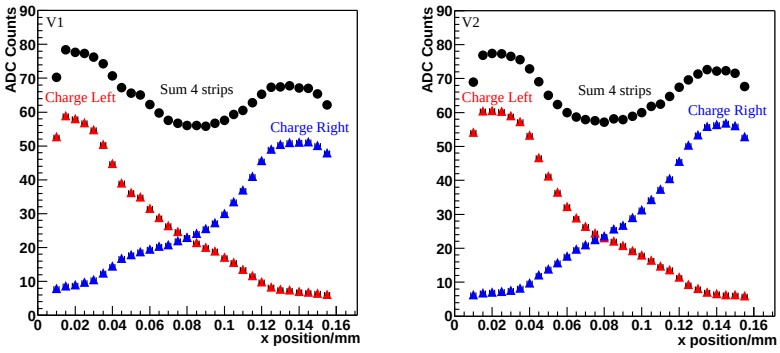

Figure 32: Charge sharing and loss for the GLAST ladder, Vfs = 400 mV.

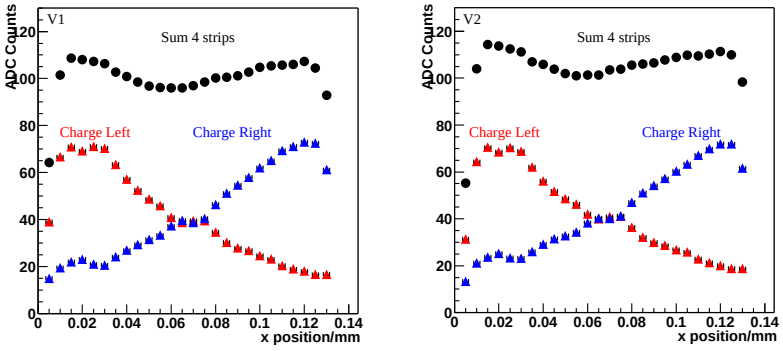

Figure 33: Charge sharing and loss for the CMS ladder, Vfs = 400 mV.

9 Conclusions

Results of measurements on prototype ladders for the LHCb Silicon Tracker in a laser setup have been presented. The setup has allowed a fast characterization of the performance of the ladders. In the future the results presented here will be compared to both simulation and to testbeam data.

For future measurements with the laser setup one area that needs improving is the time stability of the pulse height. Alternatively one of the other outputs from the beam-splitter could be monitored with time and used to correct the measured signal for time dependent drifts.

References

[1] The LHCb Collaboration. Inner Tracker Technical Design Report. CERN/LHCC 2002-029.

[2] N. van Bakel *et al.* Performance of the Beetle Readout Chip for LHCb. Proc. 8th workshop on Electronics for LHC Experiments, Colmar France, September 9-13, 2002.

[3] J. Gassner *et al.* Capacitance measurements on silicon micro-strip detectors for the TT station of the LHCb experiment. *LHCb-note*, (In preparation).

[4] S. Shaheen *et al.* Characterization and quality control of silicon microstrip detectors with an infra-red diode laser system. *NIM*, A352:573–578, 1995.

[5] I. Abt *et al.* Characterization of silicon microstrip detectors using an infra-red laser system. MPI-PhE/98-13.

[6] C. Bauer *et al.* Characterization of Inner Tracker silicon prototype sensors using a 106 Ru-source and a 1083 nm laser system. *LHCb-note*, (121), 2001.

[7] N. van. Bakel et al. The Beetle Reference Manual -chip version 1.2. *LHCb-note*, (055), 2002.

[8] Y. Ermoline. Vertex Detector Electronics: ODE Pre-Prototype. *LHCb-note*, (057), 2001.

[9] M. Agari *et al.* Test Beam Results of Multi-Geometry Prototype Sensors for the LHCb Inner Tracker. *LHCb-note*, (58), 2002.

[10] St. Heule. Simulation und Messung von Silizium Streifen-Detektoren. Master's thesis, Physik-Institut der Universität Zürich, 2003.

[11] M. Needham. Silicon Tracker Simulation Performance. *LHCb-note*, (015), 2003.